Korean J. Chem. Eng., 37(4), 707-715 (2020)
DOI: 10.1007/s11814-019-0442-4

pISSN: 0256-1115
eISSN: 1975-7220

Zwitterion imprinted composite membranes with obvious antifouling character for selective separation of Li ions

Yao Lu*, Dongshu Sun*,,***,†, Yang Lu*, Yongsheng Yan*, and Bo Hu*,†**

*Key Laboratory of Preparation and Applications of Environmental Friendly Materials (Jilin Normal University), Ministry of Education, Changchun, 130103, China
**Key Laboratory of Environmental Materials and Pollution Control, the Education Department of Jilin Province, Jilin Normal University, Siping, 136000, China
***College of Environmental Science and Engineering, Jilin Normal University, Siping, 136000, China
(*Received 4 October 2019 • accepted 24 November 2019*)

Abstract−A surface hydrophilic and antifouling imprinted composite membrane based on zwitterion and dopamine for selective adsorption Li^+ from compound has great potential. We investigated the selective adsorption amount for lithium from high Mg^{2+} and low Li^+; the resulting displayed both excellent adsorption amount of Li^+ and high selective adsorption efficiency of the fabricated membranes from the compound. Relatively lower contact angle of 50.7° and higher membrane flux value of 11.78 mL cm^{-2} min^{-1} were obtained, which indicated the imprinted composite membrane possessed high hydrophilicity. In the BSA protein adsorption experiments, the anti-pollution performance of the imprinted composite membrane was greatly improved. Moreover, the results on perm-selectivity and regeneration ability are 8.94 and 91.4%. Overall results suggest that zwitterion and dopamine can be considered effective for increasing the hydrophilicity and anti-pollution capacity. Moreover, the imprinted composite membranes could be used for selective adsorption of Li^+ effectively.

Keywords: Antifouling, Membrane Separation, Selective Separation, Zwitterion, Li^+

INTRODUCTION

Membrane separation technology has drawn great attention for separation technology by virtue of its high performance, energy saving, environmental protection and so on [1-5]. However, its fouling due to the proteins or solute in water deposition on the membrane surface, resulting in a decline in the membrane flux and service life of the membrane, remains a critical issue to be resolved [6,7].

In previous studies, increasing the hydrophilicity of the membrane can enhance the fouling resistance and reduce the mass transfer resistance [8,9]. In the meantime, surface modification is commonly used to improve hydrophilicity, which changes the contact surface involved in the separation without affecting the physical and chemical structure of the membrane [10-13]. In recent years, some approaches to preparing hydrophilic membrane by creating inorganic nanoparticles such as TiO_2, SiO_2, ZnO, GO [14-18] have been applied. However, the stability of nanoparticles on the membrane surface can easily fall off, making the membrane pores blocked. Therefore, surface chemical modification has attracted more and more attention.

As a new type of surface hydrophilic materials, the zwitterionic can react with both acids and bases in solution, while possessing positive and negatively charged dipole ions [19,20]. The zwitterionic group modified membrane material has been widely applied for the modification of polymeric membrane materials in order to obtain high water permeability across the membrane as well as in improving antifouling characteristics of membrane materials [21-23]. For the poly(sulfobetaine methacrylate) zwitterionic polymer tethered onto polypropylene membrane surface, a water contact angle of as low as 17.4° and good anti-protein-fouling performance was obtained [24]. The functionalized PVDF membrane with zwitterionic polymer brushes could not only significantly reduce flux decline, but also endow with "self-cleaning" property releasing absorbed foulants [25]. Zwitterionic membrane was fabricated by grafting 1, 3-propanesultone obtaining a high permeability of 14.6 Lm^{-2} h^{-1} bar^{-1}, high ERY rejection and low NaCl rejection, antifouling property and long-term stability [26]. Furthermore, as a biomimetic material, not only can dopamine improve the hydrophilicity, but also firmly fix the zwitterion on the surface of the membrane.

In this study, we performed a comparative study of the antifouling performance of surface modification membrane and non-surface modification membrane and the separation performance of imprinted composite membrane and non-imprinted membrane. We used Li^+ as template ion and 1,3-propane sultone as zwitterionic hydrophilic materials, synthesized zwitterion imprinted composite membranes to selectively separate of Li^+.

EXPERIMENTAL

1. Materials and Instrumentation

1-1. Materials

Polyvinylidene fluoride (PVDF) was purchased from Arkema,

†To whom correspondence should be addressed.
E-mail: 1811003@jlnu.edu.cn

France. Polyvinylpyrrolidone (PVP-K30) was purchased from Aladdin Reagent. N,N-dimethylacetamide (DMAC), N,N-dimethylformamide (DMF), N,N-dimethylethylenediamine (DMDA), 1,3-propane sultone, Tris-HCl, dopamine (DA), 2-methylol-12-crown-4 (2M12C4), 3-methacryloxypropyltrimethoxysilane (MPTS), ethylene glycol dimethacrylate (EGDMA), olefin Propyl bromide, hydroquinone, sodium carbonate (Na_2CO_3), sodium hydroxide (NaOH), azobisisobutyronitrile (AIBN) lithium chloride (LiCl), sodium chloride (NaCl), potassium chloride (KCl), Magnesium chloride ($MgCl_2$), calcium chloride ($CaCl_2$), and methanol were purchased from Sinopharm Group Chemical Reagent. The experimental water was double distilled water.

1-2. Instruments

All-digital nuclear magnetic resonance spectrometer (NMR), field emission scanning electron microscope (SEM), contact angle measuring instrument (KSV), atomic absorption spectrophotometer (ASS), The X-ray Photoelectron Spectroscopy (XPS) model is SCALAB 250XI, Thermo Fisher, USA.

2. Methods

2-1. Preparation of 2AM12C4

2M12C4 (1.0 g, 5.0 mmol), allyl bromide (0.73 g, 6.0 mmol), Na_2CO_3 (2.65 g, 25 mmol), a mixed solution of hydroquinone, iodine (micro), and anhydrous DMF (50 mL), which protected with nitrogen and heated in the dark at 71 °C for 25 h. Evaporation of the solvent in vacuo gave the crude product. By silica gel column chromatography (2.0 g, 77.5%) (methanol/dichloromethane=1 : 40, Rf= 0.2) for separation and purification products. Get ligand vinyl functionalized 12-crown-4 (2AM12C4).

2-2. Preparation of PVDF Membrane and pDA @ PVDF Membrane

(1) 4.0 g of PVDF powder, 25 mL of DMAc and 0.1 g of PVP were mixed in a three-necked round-bottomed flask to prepare a casting solution. The casting liquid was sealed and mechanically agitated at 25 °C for 24 h, keeping the temperature unchanged for 24 h to eliminate bubbles. Next, the casting solution was poured on a film applicator to set the film thickness, and then the glass plate was immersed in deionized water to prepare a PVDF film through a phase inversion process. After the phase inversion process was complete, the resulting PVDF membrane was stored in deionized water.

(2) pDA modified PVDF membrane process: First, the PVDF membrane was soaked in a pH=8.5 Tris-HCl (50 mL, 10 mM) aqueous solution for 5.0 min. Then, 100 mg of DA was added to the above solution to start the self-polymerization reaction. Under continuous mechanical shaking at room temperature, the self-polymerization process continued for 6.0 h and a thin layer of pDA was formed on the surface of the PVDF membrane. Finally, the pDA@ PVDF membrane was washed with deionized water to wash away excess pDA particles and unreacted DA.

2-3. Preparation of Zwitterionic Membrane (ZiMs)

(1) We added 10 mL of 2.0 mg mL^{-1} DMDA to 50 mL of 10 mM Tris-HCl solution, adjusted the pH of the solution to 8.5 with NaOH, immersed the above-prepared pDA@PVDF membrane in the above mixed solution at 30 °C. Magnetic stirring for 24 h. Afterwards, the prepared membrane was rinsed with deionized water to rinse off excess DMDA and Tris-HCl.

(2) 0.5 g of 1,3-propane sultone was added to 50 mL of methanol and homogenized by ultrasonication. The membrane prepared above was immersed in the above mixed solution and magnetically stirred at 30 °C. for 24 h. Afterwards, the prepared membrane was rinsed with deionized water and the excess 1, 3-propane sultone and methanol were rinsed off?the ZiMs were obtained. The synthetic route is shown in Fig. 1.

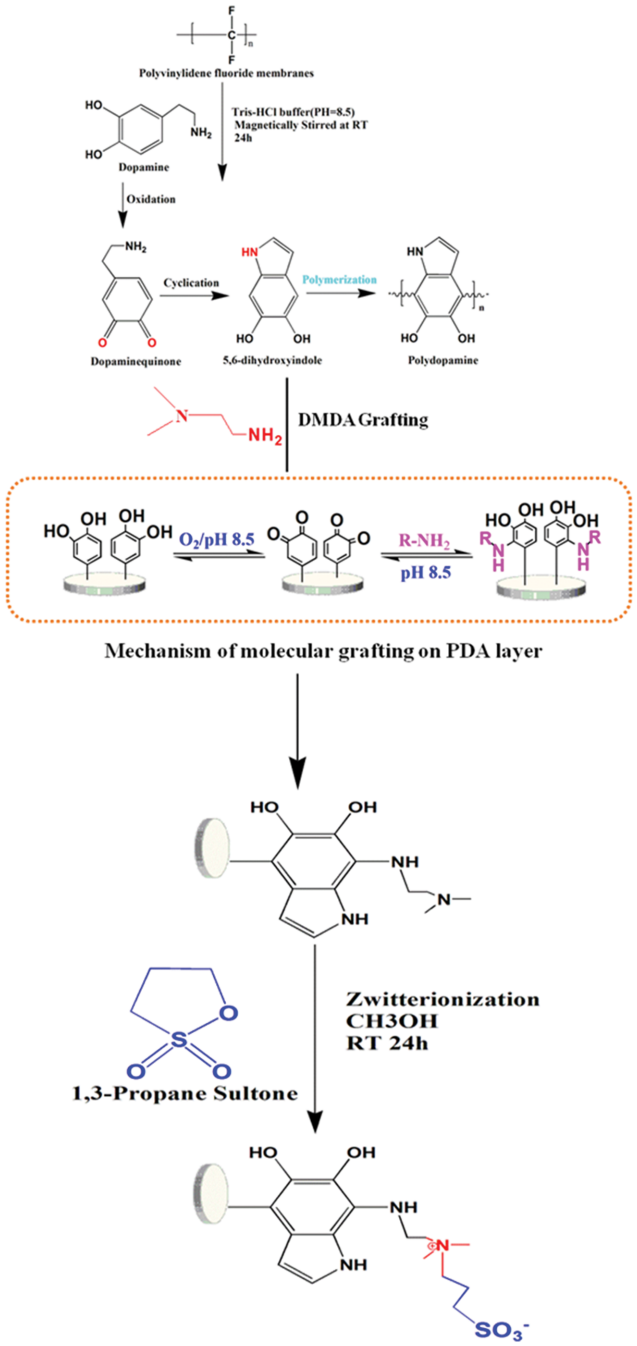

Fig. 1. Schematic of ZiMs.

2-4. Preparation of Zwitterionic Imprinted Composite Membrane (ZiIMs)

(1) The above-prepared ZiMs were first modified with MPTS, and a polymerizable double bond was introduced for further blotting. ZiMs and 2.0 mL MPTS were added to a 60 mL ethanol/water

(4 : 1, v : v) mixed solution and stirred magnetically (80 rpm) for 24 h at 80 °C. Finally, it was washed several times with ethanol and deionized water.

(2) Preparation of ZiIMs: 5.0 mmol of 2AM12C4 and 5.0 mmol of LiCl were added to 60 mL of methanol. The reaction mixture was sealed and stirred in a 25 °C water bath for 2.0 h to form a homogeneous solution. 25 mmol of MAA, 0.1 mol of EGDMA, 0.05 g of AIBN and the above-prepared film were added to the above solution in that order, and the mixture was continuously refluxed under a nitrogen atmosphere at 60 °C overnight. Finally, the resulting membrane sample was eluted with 0.5 mol L^{-1} HCl to remove Li^+ and unreacted monomer until no Li^+ was detected, and finally the membrane sample was washed with ethanol. ZiIMs were obtained after vacuum drying at 45 °C. The synthesis process of ZiNMs is similar to that of ZiIMs, except that Li^+ is not added during the synthesis.

3. Characterization of Membranes

3-1. BSA Adsorption Experiment of ZiIMs

To study the anti-contamination properties of the prepared membranes (raw PVDF membranes, pDA@PVDF, ZiMs, ZiIMs, ZiNMs), BSA was used as a template protein to study static and dynamic protein adsorption experiments. The dynamic and static adsorption experiments on BSA membranes were studied. The prepared membranes (original PVDF membrane, pDA@PVDF, ZiMs, ZiIMs, ZiNMs) (diameter 40 mm) were immersed in Tris-HCl aqueous solution (0.1 M, pH=7.4) for 5.0 min and then adsorbed onto the membrane surface with a piece of filter paper to excess Tris-HCl solution. The membrane was immersed in 50 mL of 1.0 mg mL-1 BSA aqueous solution (pH=7.4), sealed, and allowed to adsorb for 24 h at room temperature. The adsorption capacity of BSA for each membrane sample was obtained by measuring the difference in concentration of BSA solution before and after adsorption. To obtain the most accurate information for the final data, we repeated each experiment three times and calculated the average of three sets of parallel tests. At the same time, each dynamic adsorption experiment was conducted during the shaking process to evaluate the anti-contamination ability of the prepared membrane sample under simulated real conditions.

3-2. Membrane Flux Experiment of ZiIMs

The ZiIMs and the original PVDF membranes were fixed on a membrane flux testing device with an effective membrane area of 4.8 cm^2 and the membrane flux was measured at a pressure of 0.15 Mpa. The concentration of LiCl aqueous solution was 20 mg/L. The membrane flux of ZiIMs and the original PVDF membrane wasa calculated from Eq. (1):

$$J_m = \frac{V}{St} \tag{1}$$

Here, J_m (mL cm^{-2} min^{-1}) is the flux of the membrane, V (mL) is the volume of the liquid after infiltration, t (min) is the sampling time, and s (cm^2) is the effective area of the sample membrane.

3-3. Static Adsorption Experiment of ZiIMs

To measure the adsorption of Li^+ by ZiIMs and ZiNMs, adsorption isotherms and adsorption kinetics experiments were performed. The entire experimental process was performed at 25 °C. To obtain the most accurate information for the final data, we repeated each experiment three times and calculated the average of three sets of parallel tests.

3-3-1. Isothermal Adsorption Experiments of ZiIMs

In the isothermal adsorption study, one piece of ZiIMs or ZiNMs was immersed in a centrifuge tube containing 10 mL of Li^+ aqueous solution with different initial concentrations (2.0, 5.0, 8.0, 10, 15, 20, 30, 50 mg/L). It was let stand until the adsorption reached equilibrium, then the concentration of Li^+ by AAS was determined. The equilibrium adsorption capacity of ZiIMs and ZiNMs was calculated by the following formula:

$$Q_e = \frac{(C_0 - C_e)V}{m} \tag{2}$$

Q_e (mg g^{-1}) is the equilibrium adsorption capacity of ZiIMs and ZiNMs, and C_0 (mg/L) and C_e (mg/L) are the initial and equilibrium concentrations of Li^+, respectively. V (L) is the volume of the solution and m (g) is the mass of ZiIMs and ZiNMs.

3-3-2. Kinetic Adsorption Experiment of ZiIMs

Kinetic adsorption studies were performed by immersing one piece of ZiIMs or ZiNMs in a 10 mL centrifuge tube with a concentration of 10 mg/L Li^+ aqueous solution. At different time intervals (5.0, 10, 20, 30, 60, 100, 120, 180 min), the adsorbed solution was then taken out to determine the concentration of Li^+. We calculated the amount of adsorption of ZiIMs and ZiNMs at different time according to Eq. (3):

$$Q_t = \frac{(C_0 - C_t)V}{m} \tag{3}$$

Here, Q_t (mg g^{-1}) is the adsorption amount of ZiIMs and ZiNMs at different time t, C_0 (mg/L) and C_t (mg/L) are the initial concentrations of Li^+ and the concentrations at time t. V (L) is the volume of the solution and m (g) is the mass of ZiIMs and ZiNMs.

3-4. Selective Adsorption Experiment of ZiIMs

In selective adsorption experiments, Mg^{2+} was selected as the competitive ion. The ZiIMs or ZiNMs were immersed in a 10 mL mixture of Li^+ and Mg^{2+}. The Mg^{2+} concentration was 200 mg/L and the Li^+ concentrations were 2.0, 5.0, 8.0, 10, 15, 20, 30 and 50 mg/L, respectively. After adsorption reached equilibrium, the concentrations of Li^+ and Mg^{2+} samples were determined. C (mg/L) is the initial concentration of Li^+. Q_e (mg/g) is the equilibrium adsorption amount of LiIM and Mg^{2+} by ZiIMs.

3-5. Selective Penetration Experiments of ZiIMs

The permselectivity of ZiIMs and ZiNMs was tested by competitive penetration experiments. The test was in an H-type device with an effective membrane contact area of 1.5 cm^2. 100 mL of a mixed aqueous solution of Li^+ and Mg^{2+} was placed as a feed solution in the left chamber, and 100 mL of deionized water was placed as a receiving solution in the right chamber. The device was placed in a constant temperature water bath shaker to keep the solution uniform. At different time points (5.0, 15, 30, 45, 60, 120, 180 min), 5.0 mL of the received phase sample was taken to determine the ion concentration, and then 5.0 mL of water was added to the receiving phase. The final data was the average of three sets of parallel tests. Permeation flux J_x (mg cm^{-1} h^{-1}), permeability coefficient P (cm^2 h^{-1}) and selective permeability factor β are calculated by the following formula:

$$J_x = \frac{\Delta C_x V}{\Delta t A} \qquad x=Li^+, Mg^{2+} \qquad (4)$$

$$P = \frac{J_x d}{(C_{F_x} - C_{R_x})} \qquad x=Li^+, Mg^{2+} \qquad (5)$$

$$\beta_{Mg^{2+}/Li^+} = \frac{P_{Mg^{2+}}}{P_{Li^+}} \qquad (6)$$

where V, A and d represent the volume of the feed and receiving solution (mL), the effective membrane area (cm^2) and the membrane thickness, respectively. $\Delta C_x/\Delta t$ is the change in concentration in the receiving solution. $(C_{F_x} - C_{R_x})$ is the concentration difference between the feed liquid and the receiving liquid.

RESULTS AND DISCUSSION

1. Nuclear Magnetic Spectrum Analysis

The 2M12C4 modification process was analyzed by ^{1}HNMR. Fig. 2 is the ^{1}HNMR spectrum of 2M12C4(a) and 2AM12C4(b). As shown, the absorption peak at 2.02 ppm for 2AM12C4 and 2M12C4 completely disappears, and new absorption peaks appear at 5.89 ppm

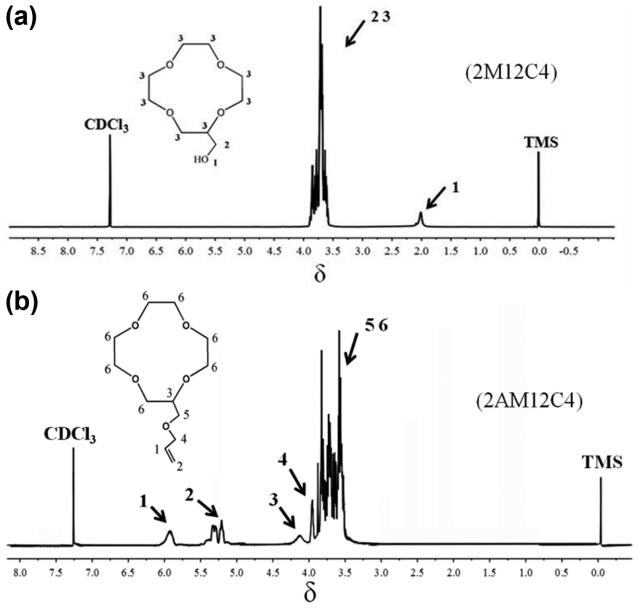

Fig. 2. ^{1}HNMR spectra of (a) 2M12C4 and (b) 2AM12C4 in $CDCl_3$.

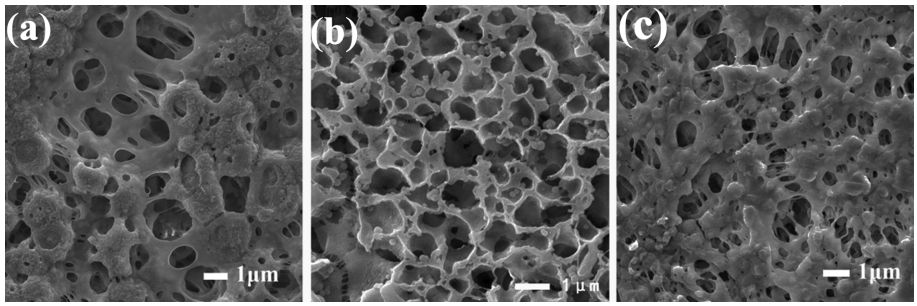

Fig. 3. Surface SEM images of (a) pristine PVDF, (b) pDA@PVDF and (c) ZiIMs.

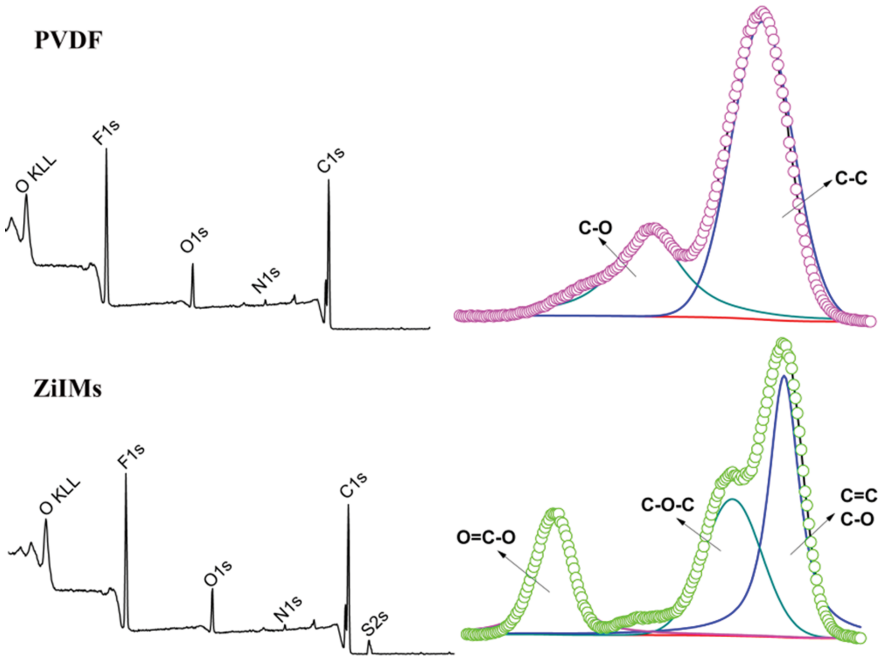

Fig. 4. XPS wide scans and narrow scans for PVDF and ZiIMs.

and 5.25 ppm, which proves that the hydroxyl group is replaced by a double bond, indicating successful synthesis of 2AM12C4.

2. SEM Analysis of Membranes

The surface morphology of pristine PVDF membrane, pDA@PVDF membrane and ZiIMs was observed by SEM. As shown in Fig. 3(a), the original PVDF film exhibits a porous and smooth film structure after the phase inversion process. Compared with the original PVDF membrane, the surface of the pDA@PVDF membrane (Fig. 3(b)) has a distinct polymer layer and a relatively rough surface structure after self-polymerization of dopamine at a slightly alkaline pH, indicating the PVDF membrane surface. The pDA layer was successfully aggregated. At the same time, as shown in Fig. 3(c), the film surface is relatively rough and the polymer layer is significantly thicker, indicating that a uniform imprinting layer was formed on the surface of the ZiIMs.

3. XPS Analysis of Membranes

The surface element composition and bonding of PVDF membrane and ZiIMs were studied by XPS broad-peak scan and peak-fitting data. As shown in Fig. 4, the broad peak scan of the PVDF membrane has F1s, O1s, N1s, and C1s peaks. Compared with PVDF membranes, after the zwitterion modification, the broad peak XPS scan of ZiIMs shows a new S2s peak, which can fully prove that the zwitterionic layer is successfully polymerized on the PVDF membrane surface. The results of fitting the C1s peaks of PVDF membranes and ZiIMs show that compared with PVDF membranes, ZiIMs fit new COC and OC=O peaks. The fitting data can fully prove that lithium ion imprinted polymers have been successfully polymerized. The surface of the film further validated the SEM results.

4. BSA Adsorption of ZiIMs

To study the antifouling properties of the prepared membranes, static and dynamic BSA adsorption experiments were conducted in detail. As shown in Fig. 5, the static adsorption of BSA in the original PVDF is close to 47.2×10^{-3} mg cm^{-2}, which is far greater than the static adsorption of BSA in other modified membranes (pDA@PVDF, ZiMs, ZiIMs, ZiNMs). The modified membrane's anti-pollution performance was greatly improved. In static and dynamic adsorption experiments, the amount of BSA adsorbed by ZiMs is lower than that of pDA@PVDF, indicating that the zwitterionic polymer layer can improve the anti-pollution ability of the film. At the same time, both ZiIMs and ZiNMs showed lower BSA adsorption, indicating that samples modified with hydrophilic surface have higher anti-pollution performance. In addition, the adsorption capacity of ZiIMs on BSA was slightly greater than that of ZiNMs, indicating that ZiNMs have higher anti-pollution capability. This may be because the surface hydrophilicity of ZiNMs is stronger during the imprinting process and is consistent with the experimental results of contact angle. Therefore, this work demonstrates that the multilayer structure of the pDA thin layer and the zwitterionic polymerization layer effectively improved the antifouling performance of the ZiIMs.

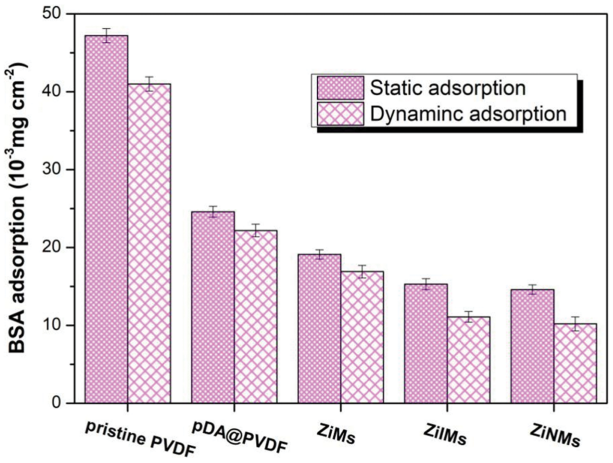

Fig. 5. BSA adsorption behaviors of various membranes under static and dynaminc.

5. Contact Angle Analysis

To study the influence of the pDA thin layer and zwitterion on the hydrophilicity of the membrane, an experiment for measuring the contact angle was studied. Note that the smaller the contact angle, the greater the hydrophilicity. The static contact angle of the film was measured by the seat drop method using a contact angle instrument. Water droplets (5.0 μm) were carefully dropped on the surface of the dry film with a microsyringe. After 10 s of dripping, imaging software was used to calculate the contact angle of the droplet. The contact angle of each film is the average of the five values measured at different locations.

The hydrophilicity of pristine PVDF membranes, pDA@PVDF, ZiMs, ZiIMs, ZiNMs was tested by measuring the static water contact angle. The results are shown in Fig. 6. The contact angle of the original PVDF film (Fig. 6(a)) is 89.7°, indicating that the original PVDF film is a hydrophobic film. Compared with the original PVDF film, the contact angle of pDA@PVDF (Fig. 6(b)) is reduced to 73.8° and the contact angle of ZiMs (Fig. 6(c)) is reduced to 54.6°. This is mainly due to the formation of pDA polymer layer and zwitterionic layer on the surface of the PVDF film, which improves the hydrophilicity of the film. In addition, the contact angle of ZiIMs (Fig. 6(d)) is 50.7°, and the contact angle of ZiNMs (Fig. 6(e)) is 50.2°, indicating that more hydrophilic layers are formed on the membrane surface during the imprinting process, improving the hydrophilicity of the membrane. The contact angles of ZiNMs are slightly smaller than those of ZiIMs. This may be because ZiIMs do not add target ions during the imprinting process and there is no elution process, so the surface is more hydrophilic. The contact angle experiment proves that the pDA polymer layer and zwitterionic modification can improve the hydrophilicity of the membrane, and further verify the experimental results of the antifouling per-

Fig. 6. Water contact angle of (a) pristine PVDF, (b) pDA@PVDF, (c) ZiMs, (d) ZiIMs and (e) ZiNMs.

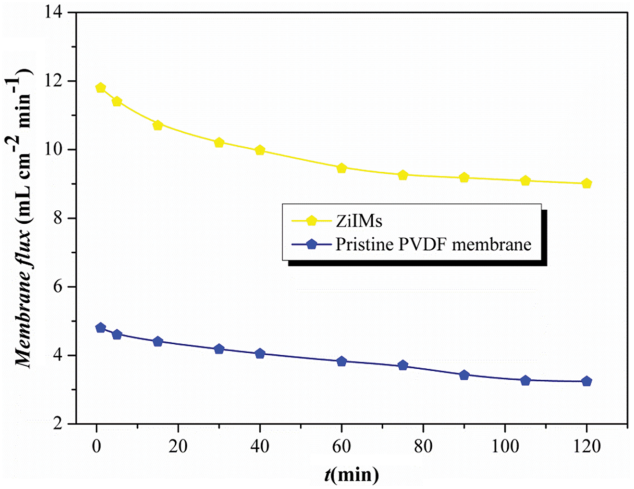

Fig. 7. Membrane flux of pristine PVDF membrane and ZiIMs.

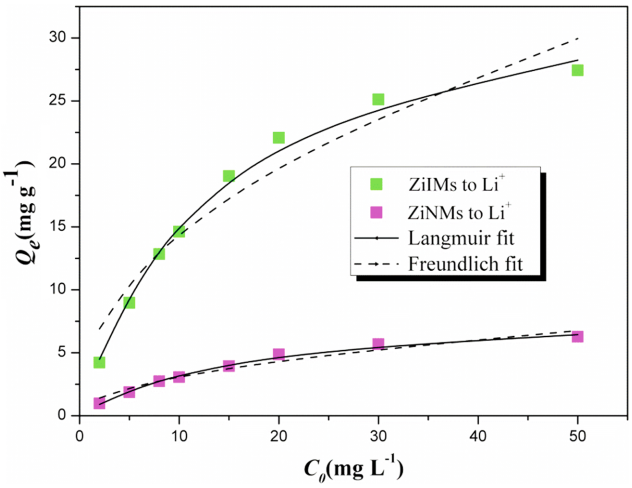

Fig. 8. Equilibrium data and Langmuir fit and Freundlich fit for the adsorption of Li^+ onto ZiIMs and ZiNMs.

formance of ZiIMs and ZiNMs.

6. Membrane Flux of ZiIMs

The original PVDF membrane and ZiIMs were fixed on the membrane flux device at a pressure of 0.15 MPa. As shown in Fig. 7, the membrane flux of the original PVDF membrane was 4.8 mL cm^{-2} min^{-1}, and the ZiIMs had a higher membrane flux of 11.78 mL cm^{-2} min^{-1}. This may be due to the pDA of the surface of the ZiIMs. The formation of polymeric layers and imprinted layers is more effective than the original PVDF membrane to identify sites; the formation of these sites is conducive to the mass transfer of Li^+.

7. Static Adsorption of ZiIMs

7-1. The Adsorption Isotherm Constants for ZiIMs

The adsorption performance of ZiIMs and ZiNMs was studied by static adsorption experiments. First, the isothermal adsorption of ZiIMs and ZiNMs was studied in detail. As shown in Fig. 8, the equilibrium adsorption capacity of ZiIMs and ZiNMs increases with the initial concentration of Li^+, and the adsorption amount of ZiIMs is significantly higher than that of ZiNMs, which may be due to the presence of a large amount of Li^+ in the surface layer of ZiIMs. Highly matched holes with specific recognition. In addition, the Langmuir and Freundlich isotherm adsorption models were used to fit the experimental data, and the adsorption mechanism of ZiIMs and ZiNMs was further explored. The formula is as follows:

$$Q_e = \frac{K_L Q_m C_0}{1 + K_L C_0} \quad (7)$$

$$Q_e = L_F C_e^{1/n} \quad (8)$$

Q_e (mg g^{-1}) is the equilibrium adsorption capacity of ZiIMs and ZiNMs. Q_m (mg g^{-1}) is the saturated adsorption capacity of ZiIMs and ZiNMs. C_0 (mg/L) is the initial solubility of Li^+ and C_e (mg/L) is the equilibrium solubility of Li^+. n is the measured surface unevenness. K_L and K_F are Langmuir and Freundlich constants, respectively.

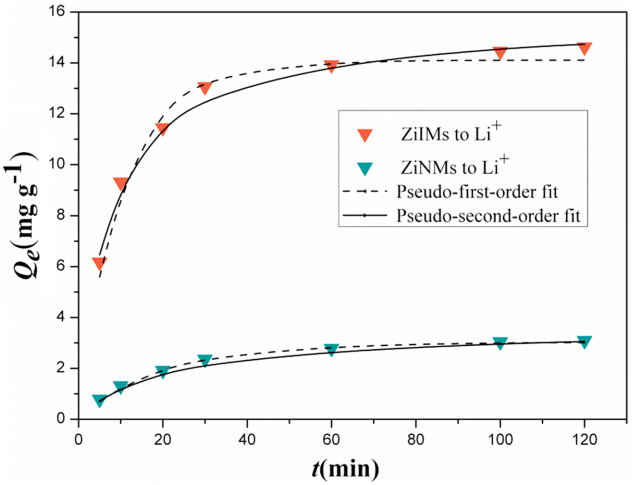

Fig. 9. Kinetic curves and fitting model for Li^+ on ZiIMs and ZiNMs.

The isothermal adsorption constants for ZiIMs and ZiNMs are listed in Table 1. As shown in Fig. 8 and Table 1, the correlation coefficient of the Langmuir model is 0.9941, and the linear regression value fits well with the Langmuir model, indicating that the adsorption process of ZiIMs is monolayer adsorption.

7-2. The Kinetics of Adsorption of ZiIMs

Secondly, the kinetic adsorption of ZiIMs and ZiNMs was studied. The kinetics of adsorption process controlled the contact time of ZiIMs and ZiNMs with the adsorption solution by 5.0-120 min. Adsorption capacity at different time t is shown in Fig. 9. The ab-

Table 1. Adsorption isotherm constants of Li^+ on ZiIMs and ZiNMs

Membranes	Langmuir Model			Freundlich modle		
	K_L	$Q_{e,cal}$	R^2	K_F	1/n	R^2
ZiIMs	0.0707	36.2226	0.9941	5.0412	0.4555	0.9324
ZiNMs	0.0583	8.6573	0.9931	1.003	0.4881	0.9502

Table 2. Pseudo-first-order and pseudo-second-order adsorption kinetic constants of Li^+ on ZiIMs and ZiNMs

Membranes	Pseudo-first-order model			Pseudo-second-order model		
	$Q_{e,cal}$	k_1 (min^{-1})	R^2	$Q_{e,cal}$	k_2 (g mg^{-1} min^{-1})	R^2
ZiIMs	14.1100	0.1011	0.9674	15.6014	0.1417	0.9931
ZiNMs	3.0197	0.0525	0.9811	3.5526	0.0598	0.9976

sorption of ZiIMs increased rapidly within the first 30 minutes, then was relatively slow, and then basically reached the adsorption equilibrium at 60 minutes. This may be due to the increased surface area of the pDA polymer layer and zwitterionic layer on the surface of the ZiIMs, exhibiting a faster adsorption rate. Compared with ZiIMs, ZiNMs exhibited a stable adsorption rate and a low equilibrium adsorption capacity, possibly due to the presence of a large number of imprinting sites on the surface of the imprinted layer of ZiIMs and specific recognition of Li^+. To study the mechanism of kinetic adsorption, kinetic adsorption data of ZiIMs and ZiNMs were fitted using a pseudo-first-order adsorption kinetics equation and a pseudo-secondary adsorption kinetics equation. The calculation formulas for the pseudo-adsorption kinetic model and the pseudo-second-order kinetics adsorption model are as follows:

$$Q_t = Q_e e^{-k_1 t} \tag{9}$$

$$Q_t = \frac{K_2 Q_e^2 t}{1 + K_2 Q_t t} \tag{10}$$

Q_e (mg g^{-1}) is the equilibrium adsorption capacity of ZiIMs and ZiNMs. Q_t (mg g^{-1}) is the amount of adsorption of ZiIMs and ZiNMs at different contact times t. K_1 (min^{-1}) and k_2 (g mg^{-1} min^{-1}) are the pseudo first-order kinetic rate constants and the pseudo-second-order kinetic rate constants.

Table 2 lists the linear regression and adsorption rate constants for the pseudo-primary and pseudo-secondary models. From Fig. 9 and Table 2, the pseudo-second-order kinetic model (R^2=0.9931) is better than the pseudo-first-order kinetic model, indicating that the adsorption kinetics of ZiIMs on Li^+ is in line with the quasi-secondary dynamics. In the model, the adsorption process is a chemical reaction process.

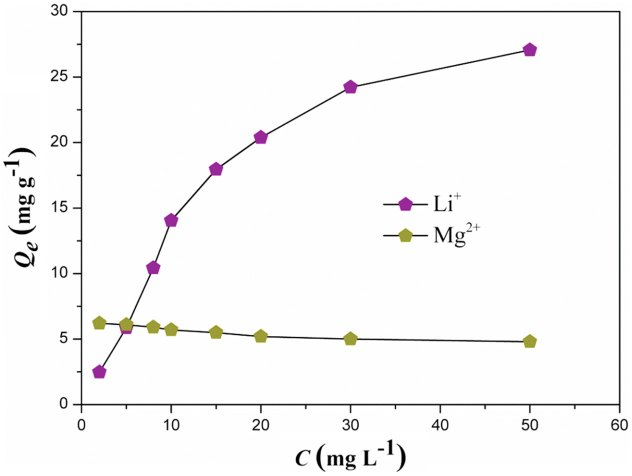

Fig. 10. Adsorption selectivity of ZiIMs.

8. Selective Adsorption of ZiIMs

To further study the selective adsorption of ZiIMs, the equilibrium adsorption capacity of ZiIMs in the high Mg^{2+}/Li^+ environment was studied. As shown in Fig. 10, as the concentration of Li^+ increases, the amount of adsorption of Li^+ by ZiIMs gradually increases, and the amount of Mg^{2+} adsorbed remains basically unchanged, which fully proves the specificity of Li^+ for high Mg^{2+}/Li^+ environments. The recognition and adsorption selectivity is good, but there is no specific selective adsorption ability for the non-template ion Mg^{2+}. This is due to the presence of specific recognition holes on the surface of ZiIMs that match the Li^+ space during

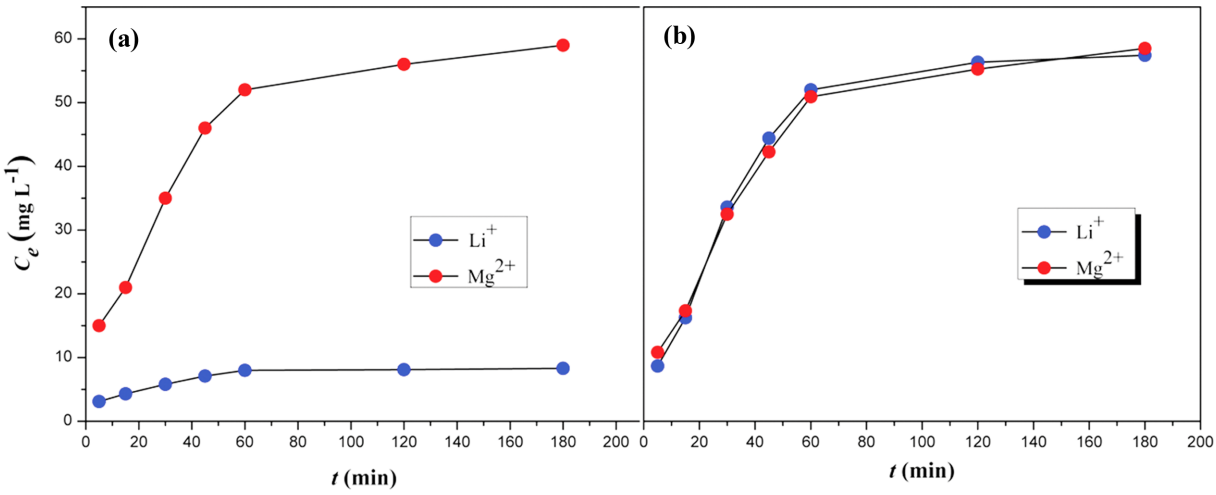

Fig. 11. The time-dependent perm-selectivity curves of Li^+ and Mg^{2+} through (a) ZiIMs and (b) ZiNMs.

Table 3. Permeation test results of ZiIMs and ZiNMs of Li^+ and Mg^{2+}

Membranes	Ions	J_x (mg cm^{-2} s^{-1})*10^{-5}	P (cm^2 s^{-1})*10^{-5}	β_{Mg^{2+}/Li^+}
ZiIMs	Li^+	6.08	0.36	8.94
	Mg^{2+}	23.71	3.22	
ZiNMs	Li^+	24.14	4.45	0.97
	Mg^{2+}	24.28	4.32	

the imprinting process, which promotes the interaction between Li^+ and ZiIMs.

9. Selective Permeation and Separation Mechanism of ZiIMs

The selective permeability of blotting membrane material is an important indicator for testing overall performance. The existence of imprinted holes on the surface of ZiIMs with specific selective adsorption of the template ion Li^+ is regarded as a Li^+ specific channel and serves the purpose of selectively separating Li^+. In this work, the selective permeation performance of ZiIMs and ZiNMs for Li^+ was studied by competitive adsorption experiments (mixed aqueous solution of Li^+ and Mg^{2+} at a concentration of 200 mg/L). The time-dependent concentration curves and permeabilities of ZiIMs and ZiNMs are shown in Fig. 11. Table 3 calculates the selective permeabilities of ZiIMs and ZiNMs for Li^+ and Mg^{2+}. As shown in Fig. 11(a), ZiIMs exhibited a higher permeation flux for the non-templated ion Mg^{2+} but a lower permeation flux for Li^+, mainly due to the presence of imprinted voids for the specific recognition of Li^+ in ZiIMs. The hole enhances the interaction between Li^+ and ZiIMs, which hinders the transmission of Li^+ on the surface of ZiIMs and allows Mg^{2+} to pass smoothly. As shown in Fig. 11(b), the permeation flux of ZiNMs to Li^+ and Mg^{2+} is almost different because ZiNMs have no imprinting effect during the synthesis and there are no imprinting holes on the surface of ZiNMs that interact with Li^+ and Mg^{2+}. ZiNMs have almost the same transmission results for Li^+ and Mg^{2+}. At the same time, the permeability factor β was 8.94, indicating that ZiIMs have excellent imprinting effect and better selectivity for Li^+ separation.

The mechanism of selective separation of ZiIMs can be summarized as two distinct approaches: (1) "Promote" permeation, combination of template with imprinted sites, preferential permeation with concentration gradient, template ion faster than other solutes; (2) "Delayed" permeation. The template interacts with the blotting sites until the adsorption at the imprinted sites is saturated, thereby impeding the template ion penetration. Due to the delay, the template ion has a slower rate of permeation than other solutes. The selective permeation results of ZiIMs indicate that ZiIMs have a higher diffusivity for Mg^{2+} than Li^+. During imprinting, the imprinted holes on the surface of ZiIMs specifically recognize Li^+, suggesting that it is difficult to recognize Mg^{2+}. Therefore, ZiIMs rarely adsorb or impede Mg^{2+} and continue to pass from one side of the ZiIMs to the other. In summary, it can be considered that the penetration process of Li^+ and Mg^{2+} through ZiIMs is a "delayed" osmotic mass transfer mechanism.

10. Regeneration and Stability Analysis of ZiIMs

Repeated adsorption and desorption cycle experiments were performed to study the reproducibility and stability of ZiIMs. The same ZiIs were used to regenerate the Li^+ solution at a concentration of 10 mg/L. ZiIMs were immersed in aqueous Li^+ solution. After the adsorption reached equilibrium, the concentration of ions in the adsorption solution was measured. The saturated ZiIMs were then eluted with 0.5 mol/L hydrochloric acid solution and the ZiIMs were further subjected to an adsorption/desorption cycle. The adsorption/desorption cycle was repeated ten times. As shown in Fig. 12, there was a decrease of only 8.6% compared with the maximum adsorption amount after ten cycles, indicating that ZiIMs can be reused many times without significant differences in adsorption capacity, indicating that ZiIMs have strong stability and reproducible performance.

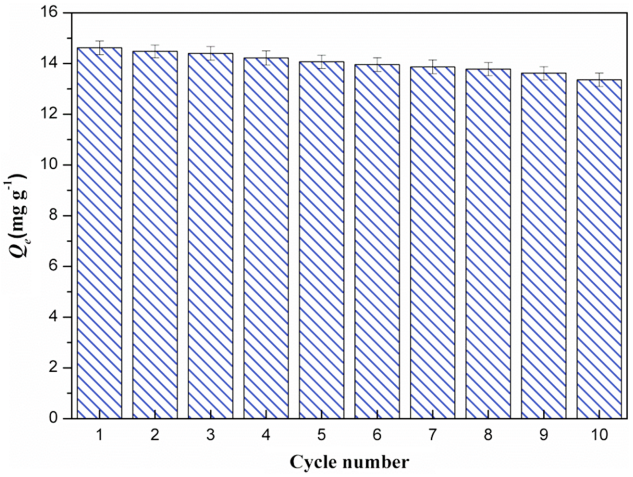

Fig. 12. Regeneration performance on the rebinding capacity of the ZiIMs.

CONCLUSION

Using PVDF membrane as substrate, a surface hydrophilic and antifouling imprinted composite membrane based on zwitterion and dopamine was synthesized. The structural composition and morphology of the imprinted membrane were studied by various characterization methods. Membrane flux tests showed that the prepared ZiIMs had good porosity, and the internal structure of the membrane was stable. The contact angle test proved that the pDA layer and the zwitterionic modified layer could improve the hydrophilicity of the membrane. The BSA adsorption experiments indicated that the anti-pollution performance of the ZiIMs was greatly improved. Static adsorption experiments showed that the prepared ZiIMs had higher adsorption capacity and faster adsorption rate. After ten adsorption/desorption cycles, the prepared ZiIMs can maintain a maximum adsorption capacity of 91.4%, indicating that

ZiIMs have good reproducible performance and stability. In summary, the membrane based on zwitterionic and dopamine surface modification has a wide application prospect in the selective separation and enrichment of Li^+.

ACKNOWLEDGEMENT

This research was supported by National Natural Science Foundation of China (21606099).

REFERENCES

1. E. Eren, A. Sarihan, B. Eren, H. Gumus and F. O. Kocak, *J. Membr. Sci.*, **475**, 1 (2015).
2. Y. Wu, M. Yan, X. Liu, P. Lv, J. Cui, M. Meng, J. Dai, Y. Yan and C. Li, *Green Chem.*, **17**, 3338 (2015).
3. J. Lu, Y. Qin, Q. Zhang, C. Yu, Y. Wu, Y. Yan, H. Fan, M. Meng and C. Li, *Chem. Eng. J.*, **360**, 483 (2019).
4. J. Lu, Y. Qin, Q. Zhang, Y. Wu, J. Cui, C. Li, L. Wang and Y. Yan, *Appl. Surf. Sci.*, **427**, 931 (2018).
5. J. Lu, Y. Wu, X. Lin, J. Gao, H. Dong, L. Chen, Y. Qin, L. Wang and Y. Yan, *J. Hazard. Mater.*, **353**, 244 (2018).
6. W. Zhang and F. Jiang, *Water Res.*, **157**, 445 (2019).
7. P. S. Goh, W. J. Lau, M. H. D. Othman and A. F. Ismail, *Desalination*, **425**, 130 (2018).
8. H. Younas, H. Bai, J. Shao, Q. Han, Y. Ling and Y. He, *J. Membr. Sci.*, **541**, 529 (2017).
9. S. Leong, A. Razmjou, K. Wang, K. Hapgood, X. Zhang and H. Wang, *J. Membr. Sci.*, **472**, 167 (2014).
10. T. D. Largier and C. J. Cornelius, *J. Power Sources*, **352**, 149 (2017).
11. D. Emadzadeh, W. J. Lau, T. Matsuura, M. Rahbari-Sisakht and A. F. Ismail, *Chem. Eng. J.*, **237**, 70 (2014).
12. Y. Wei, J. Ma and C. Wang, *J. Membr. Sci.*, **427**, 197 (2013).
13. S. R. Castrillón, X. Lu, D. L. Shaffer and M. Elimelech, *J. Membr. Sci.*, **450**, 331 (2014).
14. J. Zhang, Z. Wang, X. Zhang, X. Zheng and Z. Wu, *Appl. Surf. Sci.*, **345**, 418 (2015).
15. X. Chang, Z. Wang, S. Quan, Y. Xu, Z. Jiang and L. Shao, *Appl. Surf. Sci.*, **316**, 537 (2014).
16. M. Safarpour, A. Khataee and V. Vatanpour, *Ind. Eng. Chem. Res.*, **53**, 13370 (2014).
17. R. A. Damodar, S. J. You and H. H. Chou, *J. Hazard. Mater.*, **172**, 1321 (2009).
18. D. Sun, M. Meng, Y. Lu, B. Hu, Y. Yan and C. Li, *New J. Chem.*, **42**, 4432 (2018).
19. Y. H. Chiao, A. Sengupta, S. T. Chen, S. H. Huange, C. C. Hu, W. S. Hung, Y. Chang, X. H. Qian, S. R. Wickramasinghe, K. R. Lee and J. Y. Lai, *Sep. Purif. Technol.*, **212**, 316 (2019).
20. W. Yue, H. Li, T. Xiang, H. Qin, S. Sun and C. Zhao, *J. Membr. Sci.*, **446**, 79 (2013).
21. Q. Zhao, Q. An, Y. Ji, J. Qian and C. Gao, *J. Membr. Sci.*, **379**, 19 (2011).
22. Y. Ji, Q. An, Q. Zhao, W. Sun, K. R. Lee, H. Chen and C. Gao, *J. Membr. Sci.*, **390**, 243 (2012).
23. C. H. Worthley, K. T. Constantopoulos, M. G. Markovic, R. J. Pillar, J. G. Matisons and S. Clarke, *J. Membr. Sci.*, **385**, 30 (2011).
24. Y. Zhao, K. H. Wee and R. Bai, *J. Membr. Sci.*, **362**, 326 (2010).
25. C. Liu, D. Song, W. Zhang, Q. He, X. Huangfu, S. Sun, Z. Sun, W. Cheng and J. Ma, *Water Res.*, **168**, 115181 (2020).
26. Y. Guo, Y. Ji, B. Wu, N. Wang, M. Yin, Q. An and C. Gao, *J. Membr. Sci.*, **593**, 117441 (2020).